Design of an Exceptional-Surface-Enhanced Silicon-on-Insulator Optical Accelerometer

This article has been accepted for publication in IEEE/OSA Journal of Lightwave Technology. This is the author's version which has not been fully edited and content may change prior to final publication. Citation information: DOI 10.1109/JLT.2021.3091333

Design of an exceptional-surface-enhanced silicon-on-insulator optical accelerometer

Martino De Carlo, Francesco De Leonardis, Richard A. Soref, Vittorio M. N. Passaro

***Abstract*—Non-Hermitian photonics has attracted increasing attention especially for sensing applications. Two coupled optical systems, designed to work at the "exceptional point", exhibit a strong spectral response to perturbations. Due to the enhanced sensitivity of exceptional points, they have been usually suggested as perfect candidates for high resolution sensing. The drawback of these configurations is their undesired sensitivity also to external fluctuations and noise that could eliminate the advantages of exceptional points. Recently, the concept of exceptional surface has been proposed to overcome this problem. In particular, coupling two counterpropagating modes in the same structure prevents differential noise in distinct cavities from affecting the exceptional-point condition. In this work we present a new configuration based on exceptional surfaces to design an optical accelerometer. The strong spectral response guaranteed by exceptional surfaces is used here to demonstrate the enhancement of the sensitivity of a Bragg grating-based optical accelerometer, reaching a value of 3 nm/g at 0.5 g.**

***Index Terms*—exceptional surface, exceptional point, parity-time symmetry, anti-parity-time-symmetry, optical sensing, optical accelerometer**

I. Introduction

ACCELEROMETERS are sensors used to measure mechanical accelerations for various applications including seismic monitoring, vibration measurement and inertial navigation. Inertial navigation has especially attracted recent market interest for use in autonomous vehicles, including cars, robots and aerospace vehicles.

MEMS technology represents the state-of-the-art solution for consumer integrated accelerometers. MEMS accelerometers are one of the most popular kind of MEMS inertial sensors [1][2]. For accelerometers, several approaches have been proposed to read the displacement of a seismic mass, i.e. capacitive [3] , piezo-resistive [4], piezo-electric [5] and optical [6][7]. The capacitive approach is the one most used due to its ease of fabrication. However, optical sensing could be considered as a good alternative because of the high spatial resolution offered by optical wavelengths. Moreover, the optical approach provides intrinsic immunity against Electro-Magnetic Interferences (EMI), making it suitable to work in harsh and EMI-contaminated environments [8].

Recently a dual-axis optical MEMS accelerometer has been demonstrated using integrated Bragg gratings with a sensitivity of 30 pm/g [9] with a mass footprint of 4 mm x 4 mm. In [10], the design of a high-sensitivity optical MEMS accelerometer based on a Bragg grating integrated with a crab-leg is shown to have a sensitivity of 184 pm/g, while in [11], an optical MEMS accelerometer was demonstrated using a one-dimensional photonic crystal, providing a sensitivity of 1.17 nm/g with a core footprint of 400 μm x 400 μm. In [12], a two-dimensional photonic crystal add-drop filter has been used to demonstrate an optical MEMS accelerometer with an optical sensitivity of 0.0756 nm/g, with a 100 μm x 100 μm proof mass footprint.

In this work we propose the design of a new architecture for optical accelerometers, exploiting the concept of non-Hermitian photonics combined with integrated Bragg gratings.

Non-Hermitian photonics has attracted attention in recent research for its important property of enhanced sensitivity exhibited by exceptional points. Since Bender *et al*. discovered that non-Hermitian Hamiltonians with parity-time (PT) symmetry exhibit real spectra [13], considerable research has been conducted, especially in optics [14][15][16], dealing with whispering-gallery modes [17], coupled optical waveguides [18], optomechanics [19][20], optical gyroscopes [21][22][23][24], plasmonics [25], nanobeam cavities [26], lasers at the exceptional point [27], refractive index and absorption based sensing [28] and others. Exceptional points (EPs) are singularities in non-Hermitian Hamiltonians which exhibit a strong spectral response to perturbations because of the coalescence of two eigenstates. The resulting high sensitivity of the eigenfrequency splitting to external perturbations made EP-based devices interesting candidates for sensing purposes. In particular, the square-root dependence of the eigenfrequency splitting on parameter's perturbations at EPs is much more suitable for high resolution sensing than the linear dependence on perturbation at diabolic points [30][28]. This feature attracted the interest of researchers especially in the fields of optical sensors and even higher order non-Hermitian exceptional points have been investigated for sensing purposes [29]. However, the extraordinary sensitivity exhibited by exceptional points to external perturbations is also the reason for the particularly high influence of fabrication errors and experimental uncertainties on optical measurements [30].

Manuscript received xxx x, 2021; revised xxx x, xxxx.

M. De Carlo, F. De Leonardis, and V. M. N. Passaro are with the Photonics Research Group, Department of Electrical and Information Engineering, Politecnico di Bari, Via Orabona 4, Bari, 70126, Italy.

Richard A. Soref is with the University of Massachusetts at Boston.

Corresponding author: M. De Carlo (email: martino.decarlo@poliba.it).

The concept of exceptional surfaces (ESs) has been recently introduced with optical resonators [31] for the possibility of exploiting the extraordinary sensitivity of EPs without being subject to fabrication errors or unwanted external perturbations that would eliminate the advantage of exceptional points. Our proposed idea is to couple two counterpropagating optical modes in the same cavity. The usual exceptional point condition arising from the coupling between the two counterpropagating modes is thus called "exceptional surface" since it is maintained for any perturbation applied to the optical cavity that is common to both counterpropagating modes.

In this work we propose, for the first time, the concept of exceptional surfaces applied to an optical accelerometer. The design will consist of the arrangement of a new optical architecture able to sense the strain on a Bragg grating with increased sensitivity with respect to the simple wavelength shift in a Bragg grating strain sensor. The use of Bragg gratings to couple counterpropagating modes in optical cavities has been widely investigated and used for optical sensing [32][33]. However, by designing the system to be at the exceptional surface, it is possible to show a square-root dependence of eigenvalues on perturbation, thus providing enhanced sensitivity. Moreover, the structure proposed here makes use of two matched Bragg gratings, thus allowing compensation of the negative effect of thermal drifts.

II. Exceptional Surface Configuration

Exceptional points have been initially investigated for PT-symmetric Hamiltonians. Optical PT-symmetric Hamiltonians are usually arranged with two coupled optical resonators having identical resonances, experiencing perfectly balanced gain/loss values (one resonator has optical gain, whereas the other is lossy). The resulting eigenfrequencies are separated by a splitting proportional to the square-root of the perturbation. This is the reason for the increased sensitivity of exceptional points with respect to diabolic points [30].

However, due to the extraordinary sensitivity of exceptional points to parameter's perturbations, even unwanted small perturbations (fluctuations of the optical resonance or of the gain or loss of one of the cavities) would result in an amplified spectral response, thus cancelling all the advantages of the enhanced sensitivity. Exceptional surfaces (ESs) have been recently introduced in [31] to overcome this problem. In fact, by coupling two counterpropagating modes in the same optical resonator, rather than using two coupled modes in different resonators, it is possible to make the sensor immune to all the sources of differential perturbations applied to two distinct cavities. The basic principle for the design of an ES-based device is shown in Figure 1: one of the two optical counterpropagating modes (*e.g.* CCW) in a resonant cavity should be coupled to the other one (*e.g.* CW). In the unperturbed condition, the reciprocal coupling (CW to CCW) is absent. As soon as the perturbation κ_2 (represented by the coupling from CW to CCW modes in Figure 1) is applied, eigenfrequency splitting arises as a function of the square-root of the perturbation [31].

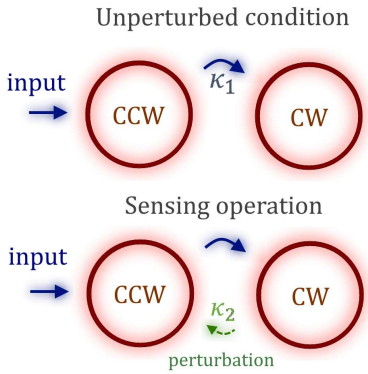

Fig. 1. Exceptional surface-based configuration illustrating schematically two waveguided modes within one microring resonator.

A. Coupled mode theory analysis

The coupled mode theory in the time domain is useful to predict the behaviour of an exceptional-surface based structure. The architecture in Figure 1 can be described with the coupled mode theory in the time domain using the effective Hamiltonian:

$$j\frac{d}{dt}\begin{bmatrix}\tilde{a}_{cw}\\ \tilde{a}_{ccw}\end{bmatrix} = H_{ES}\begin{bmatrix}\tilde{a}_{cw}\\ \tilde{a}_{ccw}\end{bmatrix}, H_{ES} = \begin{bmatrix}\omega_0 - j\gamma & \kappa_1\\ \kappa_2 & \omega_0 - j\gamma\end{bmatrix} \quad (1)$$

where $\tilde{a}_{cw}$ and $\tilde{a}_{ccw}$ are the field amplitudes of the clockwise (CW) and counterclockwise (CCW) modes, ω_0 is the optical resonance frequency of the optical cavity (same for CW and CCW modes), γ is the common loss per time unit, κ_1 (κ_2) is the coupling strength between the CCW and the CW modes (CW and CCW). The eigenfrequencies of the system are easily found, in the harmonic regime:

$$\omega_{ES_{1/2}} = \omega_0 + j\gamma \pm \sqrt{\kappa_1\kappa_2} \quad (2)$$

The maximum sensitivity of the sensor is obtained when the square-root is set to zero (the exceptional surface condition), that is, when one of the coupling strengths is zero in unperturbed conditions (as in Figure 1).

B. Scattering matrix method

The architecture proposed to realize the exceptional surface condition is shown in the dashed rectangle in Figure 2. The device is designed in the Silicon on Insulator (SOI) platform using strip waveguides with a standard cross-section (500 nm x 220 nm). A ring resonator that contains an internally located S-shaped coupling waveguide enables the unidirectional coupling of optical power from the CCW to the CW mode. The reflection r_a represents the amplitude reflection coefficient on the right part of top bus waveguide. This value represents the perturbation in our design (since it enables the coupling between the CW and the CCW modes) and will be designed to be approximatively null in unperturbed conditions, to enhance

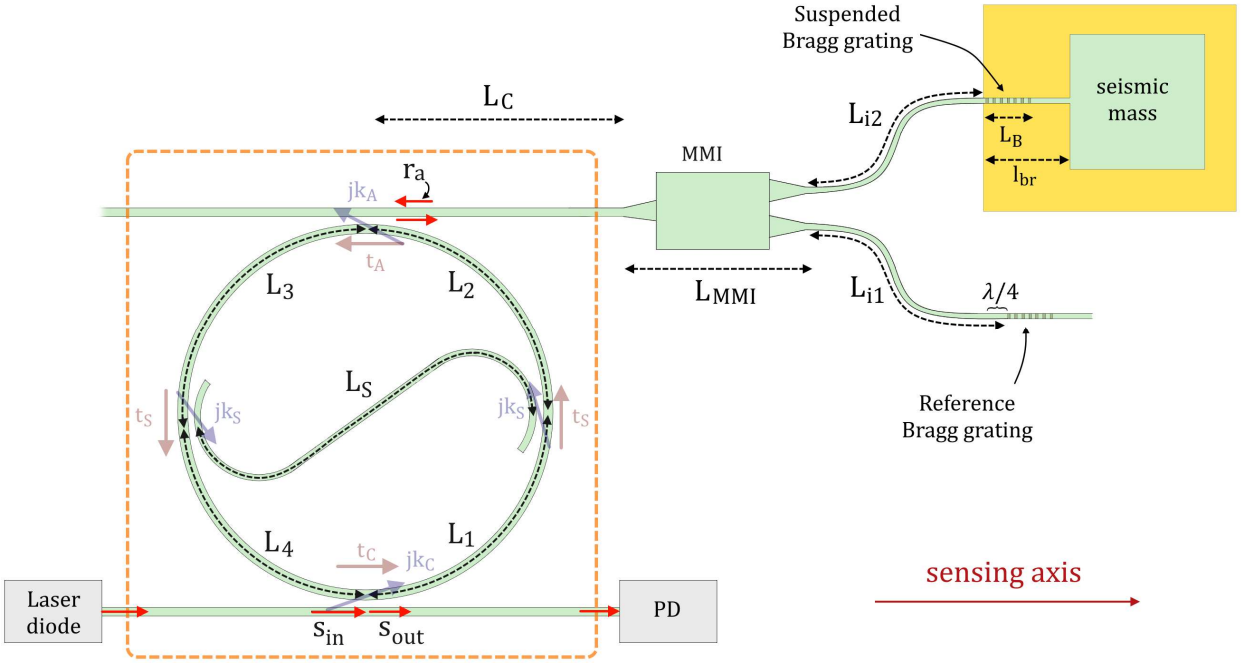

Fig. 2. Design of the exceptional-surface-based optical accelerometer. The dashed rectangle encloses the optical circuit that realizes the coupling between the CCW and the CW optical modes. The sensing axis represents the direction of the acceleration of the moving chip. The Michelson interferometer (outside the dashed rectangle), realized with an 1x2 50/50 MMI and two Bragg gratings, interferes a time-varying optical reflection (acceleration-related) with a constant optical reflection (reference).

the sensitivity.

Although the coupled mode theory in the time domain is useful to predict the behaviour of the ES-based device, to provide a more robust model to evaluate κ_1 and κ_2, a scattering matrix approach is preferred here. The scattering matrices related to the directional couplers in the dashed rectangle in Figure 2 are:

$$S_C = \begin{bmatrix} t_C & jk_C \\ jk_C & t_C \end{bmatrix} \tag{3a}$$

$$S_A = \begin{bmatrix} t_A & jk_A \\ jk_A & t_A \end{bmatrix} \tag{3b}$$

$$S_S = \begin{bmatrix} t_S & jk_S \\ jk_S & t_S \end{bmatrix} \tag{3c}$$

where t_C and jk_C are the transmission and coupling normalized amplitudes at the bottom directional coupler, t_A and jk_A are the transmission and coupling normalized amplitudes at the top directional coupler, t_S and jk_S are the transmission and coupling normalized amplitudes at the directional couplers realized with the S-shaped waveguide.

After some algebraic calculation, it can be found:

$$s_{out} = s_{in}t_C + \frac{k_C^2 s_{in} t_S (e^{j2\phi} t_A^2 t_C t_S^3 - e^{j\phi} t_A t_S - e^{j\phi}\, k_A^2 k_S^2 r_a)}{(e^{2j\phi} t_A^2 t_C^2 t_S^4 - 2e^{j\phi} t_A t_C t_S^2 - 2e^{j\phi'} k_A^2 k_S^2 r_a t_C t_S + 1)} \tag{4}$$

with $\phi = \phi_1 + \phi_2 + \phi_3 + \phi_4$, $\phi' = \phi_1 + 2\phi_3 + \phi_4 + \phi_S$ and $\phi_i = (2\pi/\lambda) n_{\text{eff}} L_k$, where $k = 1,2,3,4,S$ (lengths L_k are shown in Figure 2).

The eigenvalues are easily found by equating the denominator to zero, resulting in:

$$e^{j\phi_{ES}} = \frac{1 \pm \sqrt{2k_A k_S e^{j\phi'} r_a t_C t_S}}{j t_A t_C t_S^2} \tag{5}$$

The eigenvalues splitting around the exceptional surface condition is then found to be:

$$\Delta\phi_{ES} = 2j\sqrt{2k_A k_S e^{j\phi'} t_C t_S r_a} \tag{6}$$

It is seen that the eigenvalues splitting is proportional to $r_a^{1/2}$, confirming the exceptional surface condition. Moreover, the phase of $e^{j\phi'} r_a$ should be designed to be π, during sensing operation, in order to obtain the maximum real splitting between the eigenvalues [31].

Once the architecture has been demonstrated to work at the exceptional surface, we need to synthesize the needed r_a for the specific application of an optical accelerometer.

III. Design of Exceptional-Surface Accelerometer

This section is focused on the design of an optical accelerometer. The maximum sensitivity of the ES-based sensor is obtained in the proximity of $r_a = 0$. The idea that we propose is to exploit the destructive interference between the optical signals reflected by two matched Bragg reflectors in order to obtain $r_a \cong 0$ in unperturbed conditions. We have designed the Michelson interferometer illustrated schematically in Figure 2 (outside the dashed rectangle) that interferes a time-varying optical reflection (acceleration-related) with a constant optical reflection (reference). In particular, one Bragg grating

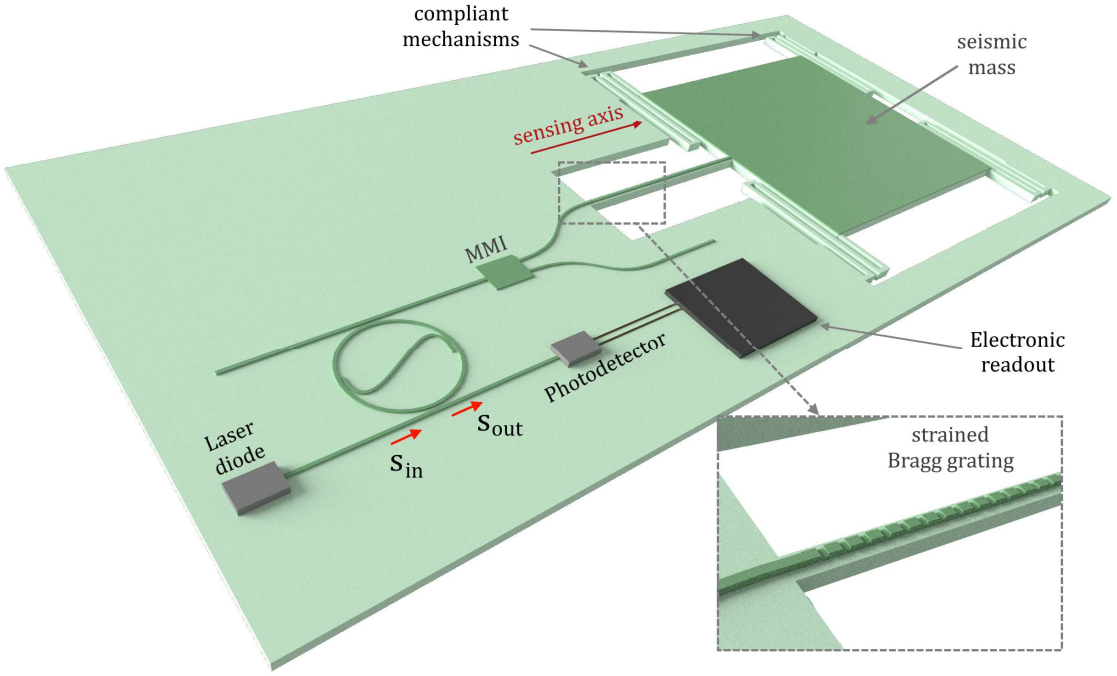

Fig. 3. Rendering of the final device. The sensing axis represents the direction of the acceleration of the moving chip.

will be suspended and will sense the strain of a seismic mass, while the second grating will be fixed in space and time. The amplitude reflectance of the structure in Figure 2 that employs a Multi-Mode Interferometer (MMI) splitter can be approximated as:

$$r_a = e^{j2\phi_c}\left(K_1^2\, e^{j2\phi_{MMI}}\, e^{j2\phi_{i1}} r_{B_1} + K_2^2 e^{j2\phi_{MMI2}}\, e^{j2\phi_{i2}} r_{B_2}\right) \quad (7)$$

with $\phi_{i1,2} = \frac{2\pi}{\lambda} n_{\text{eff}} L_{i1,2}$ and $\phi_c = \frac{2\pi}{\lambda} n_{\text{eff}} L_c$ ($L_{i1,2}$ and L_C shown in Figure 2), with $r_{B_{1(2)}}$ the amplitude reflection coefficient of the first (second) Bragg grating and $K_{1(2)} e^{j\phi_{MMI1(2)}}$ the amplitude transmission coefficient of the MMI from input port to the first (second) output port.

The 1 x 2 50/50 MMI has been simulated with a propagator software for an operating wavelength of 1.535 µm. The MMI coupler length is 31.8 µm, whereas the width is 6 µm. The input and output tapers length is 20 µm, whereas their maximum width (next to the MMI coupler) is 6 µm. With simulations, it has been obtained that $K_1\, e^{j\phi_{MMI}} = K_2\, e^{j\phi_{MMI2}} = 0.687 + 0.17j$ (with $\left|K_{1(2)}\right|^2 \cong 0.48$).

By designing $\phi_{i2} = \phi_{i1} + \pi/4$ at the operating wavelength, we obtain the destructive interference between the two optical signals reflected by the Bragg gratings, thus making $r_a \cong 0$ at the operating wavelength.

The final configuration of the device is shown in Figure 3 where the tunable laser light source and the photodetector diode can both be on-chip in principle. The seismic mass represents the inertial element causing a strain-induced perturbation of the suspended Bragg grating connected to it. The perturbation of the suspended strained Bragg creates a mismatch (both in the period of the grating and of the refractive index of the strained materials) with respect to the reference Bragg grating. The fabrication of the proposed device can use the same micromachining technique proposed in [9]. The wafer to be used should be a standard SOI wafer with a buried 2 µm silicon dioxide layer. The residual silicon substrate in the seismic mass region, after micromachining will be of about 20 µm thickness, while the substrate Si is completely removed under the suspended Bragg grating. The seismic mass is designed to have a footprint of 400 µm x 400 µm.

A. *Bragg Grating modelling*

The Bragg grating is obtained by locally etching the optical waveguide by a depth d_B, with an unperturbed period Λ_0 and a duty cycle DC. Bragg grating reflectors have been modelled as proposed in [34] and [35]. In particular, the amplitude reflection coefficient of each Bragg grating is given by the following expression:

$$r_B = -\frac{j\kappa^* \sinh(\gamma_B L_B)}{\gamma_B \cosh(\gamma_B L_B) + j\delta \sinh(\gamma_B L_B)} \quad (8)$$

where

$$\gamma_B = \sqrt{|\kappa|^2 - \delta^2} \quad (9a)$$

$$\delta = \frac{2\pi n_{\text{eff}}}{\lambda} - \frac{2\pi}{\Lambda_0} = 2\pi n_{\text{eff}}\left(\frac{1}{\lambda} - \frac{1}{\lambda_B}\right) \quad (9b)$$

$$\kappa = \frac{j\pi}{2P\lambda\eta_0} \int_{grating} (n_{\text{core}}^2 - n_{\text{clad}}^2) |\boldsymbol{E}|^2 dxdy \frac{\sin(\pi DC)}{\pi} \quad (9c)$$

with λ the operating wavelength, P the optical power of the mode, η_0 the vacuum impedance, n_{core} the effective index of

TABLE I
BRAGG GRATING PARAMETERS

Parameter	Value
$\|\kappa\|$	459.36 cm^{-1}
L_B	50 μm
DC	0.15
Λ_0	1.535 μm
d_B	20 nm

the core (etched material) and n_{clad} is the material of the cladding (air in this case). A value of κ of 459.36 cm^{-1} has been estimated from simulations in COMSOL Multiphysics. Figure 4 shows the fundamental TE optical mode in the non-etched cross section of the Bragg grating. Figure 5 shows the optical spectrum of the designed Bragg grating with the parameters of Table I.

The effect of the acceleration-induced strain on the suspended Bragg grating can be modelled, by means of two distinct effects upon the Bragg grating:

-change of the period of the grating

-photoelastic change in the refractive index of the strained materials.

The perturbed period of the Bragg grating can be evaluated as:

$$\Lambda = \Lambda_0(1+\epsilon) \tag{10}$$

with ϵ the mechanical strain on the Bragg grating.

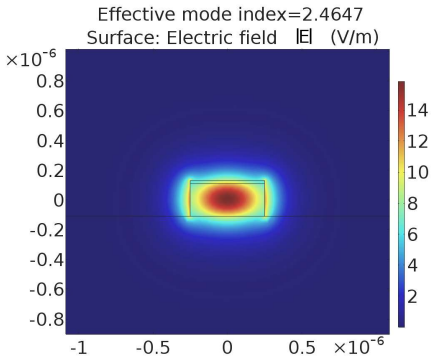

Fig. 4. Optical mode calculated for a standard 500 nm x 220 nm SOI strip waveguide cross section.

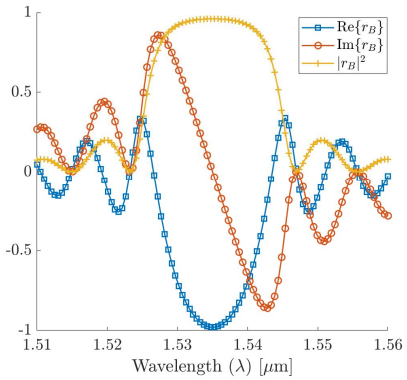

Fig. 5. Modelled unperturbed Bragg spectral response as a function of the wavelength.

whereas the change of refractive index of strained materials could be accounted as:

$$\Delta n = -\frac{1}{2}n^3 p_{lm}\epsilon \tag{11}$$

where p_{lm} is the component of the photoelastic tensor along the sensing direction. For this Bragg grating with a Silicon core, the effect of the photoelastic effect is negligible for any of the considered components of the photoelastic tensor with respect to the effect on the perturbation of the grating period, as in [9].

B. *Mechanical modeling*

In order to model the device, we need to relate the acceleration of the seismic mass to the strain induced in the Bragg grating bridge. The Bragg grating bridge can be modelled using the spring constant along the sensing direction:

$$k_B = \frac{EA_B}{l_{br}} \tag{12}$$

where E is the Young's modulus (weighted on the cross-section areas of different materials comprising the Bridge) of the bridge material, A_B is the cross-sectional area of the Bridge, and l_{br} is the length of the waveguide bridge. The width of the SiO_2 bottom cladding of the device is designed to be 3 μm. Due to the much higher area occupied by the SiO_2 bottom cladding (2 μm x 3μm) with respect to the Si core (220 nm x 500 nm), the spring constant of the Bragg bridge is mostly determined by the SiO_2 part. The approximated parameters used to model the spring constant of the Bragg grating bridge are summarized in Table II.

The spring constant along the sensing axis for each of the four compliant spring mechanisms (k_p) (see Figure 3) has been evaluated via COMSOL Multiphysics to be 2-to-3 orders of magnitude lower than the k_B.

The total spring constant along the sensing axis is:

$$k_y = k_B + 4k_p \cong k_B \tag{13}$$

The mechanical resonance frequency f_0 of the device is given by [36]:

$$f_0 = \frac{1}{2\pi}\sqrt{\frac{k_y}{m}}, \tag{14}$$

where m is the seismic mass.

Finally, the relative strain on the Bragg grating bridge ($\epsilon = \Delta l_{br}/l_{br}$) at an acceleration a along the sensing axis is [36]:

$$\epsilon = a\frac{m}{k_y l_{br}} \tag{15}$$

The mechanical parameters used for the simulations are summarized in Table II.

This article has been accepted for publication in IEEE/OSA Journal of Lightwave Technology. This is the author's version which has not been fully edited and content may change prior to final publication. Citation information: DOI 10.1109/JLT.2021.3091333

TABLE II
MECHANICAL PARAMETERS

Parameter	Value
l_{br}	200 µm
A_B	10,11 µm^2
E_{Si}	170 GPa
E_{SiO_2}	66 GPa
d_{Si}	2.33 g/cm^3
d_{SiO2}	2.65 g/cm^3
k_y	2.077 kN/m
f_0	2.51 kHz
V	400 x 400 x 22.22 µm^2
m	8.38 µg

IV. RESULTS

Table III summarizes the parameters used for the final numerical simulation. Figure 6 shows the normalized spectral response for different values of the acceleration a (as fractions of gravity acceleration g). The top left figure shows the resonance dip in the unperturbed condition. For an applied acceleration of 0.25 g, only a broadening of the resonance dip is visible. Whereas, starting from a = 0.5 g, a splitting between the resonance dips is observed. Then, the higher the acceleration, the greater the splitting between the resonance dips. It should be noticed that the splitting measured on the spectral response (Figure 6) doesn't strictly correspond to the eigen-wavelengths splitting, especially for small values of the acceleration, due to the overlapping of the two resonance dips. Consequently, although the splitting between the resonance dips appears only at 0.5 g, even smaller accelerations can be detected if a regression method is used to the detect the eigenvalues splitting from Figure 6.

Figure 7 shows the resonance splitting measured on the output spectrum of the ES-based accelerometer ($\Delta\lambda_{ES}$) as a function of the ratio a/g. In the same figure, the variation of the central wavelength of the Bragg grating $\Delta\lambda_B$ with respect to the unperturbed Bragg grating central wavelength is shown, thus demonstrating the increase of about one order of magnitude in the splitting of the proposed device, with respect to a simple Bragg grating strain sensor.

TABLE III
FINAL DESIGN PARAMETERS

Parameter	Value
L_1	48.75 µm
L_2	48.75 µm
L_3	48.75 µm
L_4	48.75 µm
L_S	97.48 µm
L_{i1}	10 µm
L_{i2}	10.015 µm
L_C	10 µm
t_C	0.53
t_A	0.14
t_S	0.14

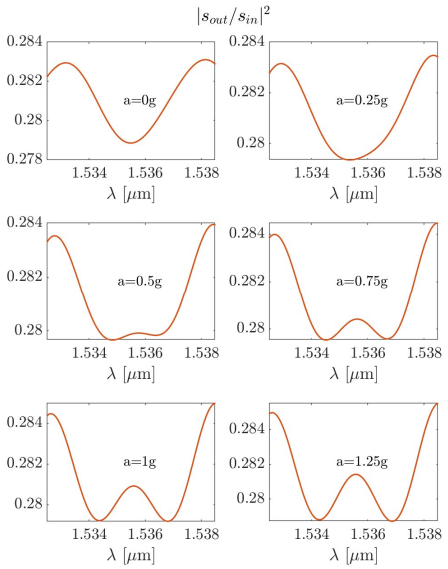

Fig. 6. Spectral output of the transfer function $|s_{out}/s_{in}|^2$ as a function of wavelength for different values of the acceleration a.

This represents the main result of this work: with the proposed configuration, the resonance splitting obtained with the exceptional surface-enhanced configuration can be one order of magnitude higher than the wavelength shift obtained with a standard Bragg grating, without the need of external gain.

For the designed system, the differential sensitivity ($d\Delta\lambda/da$) has been evaluated to be 3 nm/g at 0.5 g acceleration.

To determine the acceleration, the wavelength of the tunable laser source should be scanned across the wavelength range of interest, which here is 1.533 µm to 1.538 µm. Then, for the electronic readout, the measured photocurrent should be processed by an electronic Digital Signal Processor (DSP), that can use a method of regression (for example, the "Ordinary Least Squares" method) to fit the spectrum and to predict the real eigen-wavelength splitting (the same method of fitting is often used to predict the real and the imaginary parts of the eigenfrequencies in PT-symmetric systems).

The designed device is proposed on a purely passive platform (SOI). However, using a platform where gain is available,

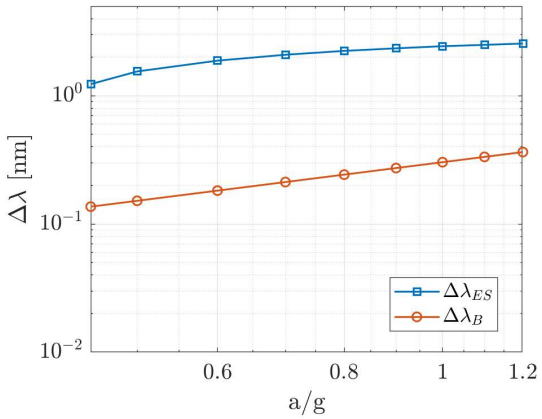

Fig. 7. Spectral splitting ($\Delta\lambda_{ES}$) at the exceptional surface as a function of the relative acceleration a/g, evaluated as the distance between the resonance dips.

(waveguided semiconductor optical amplifier) sharper resonances could let much smaller resolutions be achieved, thus enabling high resolution acceleration sensing, even with very small seismic mass. In this way a further enhancement of an optical accelerometer could be achieved.

While our proposal showed an enhanced sensitivity with respect to a Bragg-grating-based accelerometers [9][10], there are other promising techniques exploiting high-finesse cavities and photonic bandgaps.

The solution fabricated in [37] shows a high optical sensitivity (90 nm/g), with a small measurement range (±0.263 g) and a low first mechanical resonant frequency (438 Hz).

In contrast, the one dimensional and two dimensional photonic-bandgap-based accelerometers in [11] and [12] have been numerically demonstrated to have linear sensitivities of 1.17 nm/g and 0.0756 nm/g and first mechanical resonances of 8.9 kHz and 12.9 kHz, respectively. Both these solutions have high measurement ranges (±22 g in [11] and ±156 g in [12]).

A benefit of the configuration proposed here with respect to high-finesse solutions is that it does not require a very stable laser source or active locking techniques. Moreover, in principle, the solution proposed here could exhibit a very high dynamic range, thanks to the square root dependence of the splitting on the acceleration. However, the same intrinsic square-root behavior worsens the splitting enhancement for high values of the acceleration with respect to a classical Bragg-grating-based accelerometer, thus making it difficult to perform a fair comparison with the dynamic ranges of the different solutions. In this work, we have numerically evaluated that the splitting enhancement of the proposed accelerometer at the exceptional surface is absent for values of the acceleration higher than 10 g.

We want to underline that the aim of this work was to demonstrate the high possibility of the exceptional surface to enhance the sensitivity of an optical accelerometer, compared with that of the standard Bragg-grating-based accelerometer, for small values of acceleration. Moreover, the possibility of combining the exceptional surface with the photonic bandgap or with the accelerometer implemented with optical gain, could easily lead to better performances.

V. Conclusion

In this paper we have designed an optical accelerometer based on exceptional surfaces. The square-root dependence of the eigenfrequency splitting on perturbations, typical of non-Hermitian Hamiltonians, has been exploited here to enhance the sensitivity of a strain-based Bragg grating accelerometer. The interference between a sensing suspended Bragg grating and a reference Bragg grating allows the condition of exceptional surface to be obtained. The advantage of the proposed solution is the use of exceptional surfaces, rather than exceptional points, to realize the non-Hermitian Hamiltonian. By coupling two counterpropagating modes of a single optical resonator, it is possible to overcome all the noise problems of PT-symmetric sensors related to the unwanted differential perturbations applied on distinct cavities. The proposed configuration has been designed for the Silicon on Insulator platform, thus demonstrating that no gain is necessary to obtain the desired sensitivity enhancement. A sensitivity of 3 nm/g has been achieved at 0.5 g acceleration. However, a design with the integration of optical gain could give sharper resonances in the optical response, thus reaching even greater sensitivity.

References

[1] W. Fleming, "Overview of automotive sensors", *IEEE Sensors Journal*, vol. 1, no. 4, pp. 296-308, 2001. Available: 10.1109/7361.983469.

[2] J. Judy, "Microelectromechanical systems (MEMS): fabrication, design and applications", *Smart Materials and Structures*, vol. 10, no. 6, pp. 1115-1134, 2001. Available: 10.1088/0964-1726/10/6/301.

[3] H. Xie and G. Fedder, "Vertical comb-finger capacitive actuation and sensing for CMOS-MEMS", *Sensors and Actuators A: Physical*, vol. 95, no. 2-3, pp. 212-221, 2002. Available: 10.1016/s0924-4247(01)00740-3.

[4] R. Amarasinghe, D. Dao, T. Toriyama and S. Sugiyama, "Development of miniaturized 6-axis accelerometer utilizing piezoresistive sensing elements", *Sensors and Actuators A: Physical*, vol. 134, no. 2, pp. 310-320, 2007. Available: 10.1016/j.sna.2006.05.044.

[5] S. Tadigadapa and K. Mateti, "Piezoelectric MEMS sensors: state-of-the-art and perspectives", *Measurement Science and Technology*, vol. 20, no. 9, p. 092001, 2009. Available: 10.1088/0957-0233/20/9/092001.

[6] D. Tang, D. Zhao, Y. Wang, X. Zhang, Z. Liang and F. Guo, "A MOEMS accelerometer based on photoelastic effect", *Optik*, vol. 122, no. 7, pp. 635-638, 2011. Available: 10.1016/j.ijleo.2010.02.031.

[7] T. Yoshino, Y. Sano, D. Ota, K. Fujita and T. Ikui, "Fiber-Bragg-Grating Based Single Axial Mode Fabry-Perot Interferometer and Its Strain and Acceleration Sensing Applications", *Journal of Lightwave Technology*, vol. 34, no. 9, pp. 2241-2250, 2016. Available: 10.1109/jlt.2016.2521440.

[8] T. Guan, G. Keulemans, F. Ceyssens and R. Puers, "MOEMS uniaxial accelerometer based on EpoClad/EpoCore photoresists with built-in fiber clamp", *Sensors and Actuators A: Physical*, vol. 193, pp. 95-102, 2013. Available: 10.1016/j.sna.2012.12.030.

[9] B. Malayappan, N. Krishnaswamy and P. Pattnaik, "Novel High-Resolution Lateral Dual-Axis Quad-Beam Optical MEMS Accelerometer Using Waveguide Bragg Gratings", *Photonics*, vol. 7, no. 3, p. 49, 2020. Available: 10.3390/photonics7030049.

[10] B. Malayappan, N. Krishnaswamy and P. Pattnaik, "Optical MEMS Accelerometer Based on Waveguide Bragg Grating Integrated with Crab-Leg Beam", *2020 IEEE SENSORS*, 2020. Available: 10.1109/sensors47125.2020.9278931.

[11] A. Sheikhaleh, K. Abedi and K. Jafari, "A Proposal for an Optical MEMS Accelerometer Relied on Wavelength Modulation With One Dimensional Photonic Crystal", *Journal of Lightwave Technology*, vol. 34, no. 22, pp. 5244-5249, 2016. Available: 10.1109/jlt.2016.2597539.

[12] A. Sheikhaleh, K. Abedi and K. Jafari, "An Optical MEMS Accelerometer Based on a Two-Dimensional Photonic Crystal Add-Drop Filter", *Journal of Lightwave Technology*, vol. 35, no. 14, pp. 3029-3034, 2017. Available: 10.1109/jlt.2017.2706140.

[13] C. Bender and S. Boettcher, "Real Spectra in Non-Hermitian Hamiltonians Having PT Symmetry", *Physical Review Letters*, vol. 80, no. 24, pp. 5243-5246, 1998. Available: 10.1103/physrevlett.80.5243.

[14] C. Rüter, K. Makris, R. El-Ganainy, D. Christodoulides, M. Segev and D. Kip, "Observation of parity–time symmetry in optics", *Nature Physics*, vol. 6, no. 3, pp. 192-195, 2010. Available: 10.1038/nphys1515.

[15] R. El-Ganainy, K. Makris, M. Khajavikhan, Z. Musslimani, S. Rotter and D. Christodoulides, "Non-Hermitian physics and PT symmetry", *Nature Physics*, vol. 14, no. 1, pp. 11-19, 2018. Available: 10.1038/nphys4323.

[16] M. Parto, Y. Liu, B. Bahari, M. Khajavikhan and D. Christodoulides, "Non-Hermitian and topological photonics: optics at an exceptional point", *Nanophotonics*, vol. 10, no. 1, pp. 403-423, 2020. Available: 10.1515/nanoph-2020-0434.

[17] B. Peng et al., "Parity–time-symmetric whispering-gallery microcavities", *Nature Physics*, vol. 10, no. 5, pp. 394-398, 2014. Available: 10.1038/nphys2927.

[18] S. Klaiman, U. Günther and N. Moiseyev, "Visualization of Branch Points in PT-Symmetric Waveguides", *Physical Review Letters*, vol. 101, no. 8, 2008. Available: 10.1103/physrevlett.101.

[19] W. Li, Y. Jiang, C. Li and H. Song, "Parity-time-symmetry enhanced optomechanically-induced-transparency", *Scientific Reports*, vol. 6, no. 1, 2016. Available: 10.1038/srep31095.

[20] M. De Carlo, F. De Leonardis, L. Lamberti and V. Passaro, "Generalized Modeling of Optomechanical Forces Applied to PT-Symmetric Optical Microscale Resonators", *Journal of Lightwave Technology*, vol. 37, no. 10, pp. 2178-2184, 2019. Available: 10.1109/jlt.2019.2899486.

[21] J. Ren et al., "Ultrasensitive micro-scale parity-time-symmetric ring laser gyroscope", *Optics Letters*, vol. 42, no. 8, p. 1556, 2017. Available: 10.1364/ol.42.001556.

[22] M. De Carlo, F. De Leonardis and V. Passaro, "Design Rules of a Microscale PT-Symmetric Optical Gyroscope Using Group IV Platform", *Journal of Lightwave Technology*, vol. 36, no. 16, pp. 3261-3268, 2018. Available: 10.1109/jlt.2018.2837754.

[23] M. De Carlo, F. De Leonardis, L. Lamberti and V. Passaro, "High-sensitivity real-splitting anti-PT-symmetric microscale optical gyroscope", *Optics Letters*, vol. 44, no. 16, p. 3956, 2019. Available: 10.1364/ol.44.003956

[24] M. Hokmabadi, A. Schumer, D. Christodoulides and M. Khajavikhan, "Non-Hermitian ring laser gyroscopes with enhanced Sagnac sensitivity", *Nature*, vol. 576, no. 7785, pp. 70-74, 2019. Available: 10.1038/s41586-019-1780-4. (2019)

[25] H. Benisty et al., "Implementation of PT symmetric devices using plasmonics: principle and applications", *Optics Express*, vol. 19, no. 19, p. 18004, 2011. Available: 10.1364/oe.19.018004.

[26] S. Zhang, Z. Yong, Y. Zhang and S. He, "Parity-Time Symmetry Breaking in Coupled Nanobeam Cavities", *Scientific Reports*, vol. 6, no. 1, 2016. Available: 10.1038/srep24487.

[27] M. Brandstetter et al., "Reversing the pump dependence of a laser at an exceptional point", *Nature Communications*, vol. 5, no. 1, 2014. Available: 10.1038/ncomms5034.

[28] M. De Carlo, "Exceptional points of parity-time- and anti-parity-time-symmetric devices for refractive index and absorption-based sensing", *Results in Optics*, vol. 2, p. 100052, 2021. Available: 10.1016/j.rio.2020.100052.

[29] H. Hodaei et al., "Enhanced sensitivity at higher-order exceptional points", *Nature*, vol. 548, no. 7666, pp. 187-191, 2017. Available: 10.1038/nature23280

[30] J. Wiersig, "Review of exceptional point-based sensors", *Photonics Research*, vol. 8, no. 9, p. 1457, 2020. Available: 10.1364/prj.396115.

[31] Q. Zhong, J. Ren, M. Khajavikhan, D. Christodoulides, Ş. Özdemir and R. El-Ganainy, "Sensing with Exceptional Surfaces in Order to Combine Sensitivity with Robustness", *Physical Review Letters*, vol. 122, no. 15, 2019. Available: 10.1103/physrevlett.122.153902.

[32] C. Campanella, M. De Carlo, A. Cuccovillo and V. Passaro, "Loss-induced control of light propagation direction in passive linear coupled optical cavities", *Photonics Research*, vol. 6, no. 6, p. 525, 2018. Available: 10.1364/prj.6.000525.

[33] C. Campanella, M. De Carlo, A. Cuccovillo, F. De Leonardis and V. Passaro, "Methane Gas Photonic Sensor Based on Resonant Coupled Cavities", *Sensors*, vol. 19, no. 23, p. 5171, 2019. Available: 10.3390/s19235171.

[34] A. Yariv and P. Yeh, *Optical waves in crystals*. Hoboken, N.J.: John Wiley and Sons, 2003.

[35] V. Passaro, R. Loiacono, G. D'Amico and F. De Leonardis, "Design of Bragg Grating Sensors Based on Submicrometer Optical Rib Waveguides in SOI", *IEEE Sensors Journal*, vol. 8, no. 9, pp. 1603-1611, 2008. Available: 10.1109/jsen.2008.929068.

[36] T. Storgaard-Larsen, S. Bouwstra and O. Leistiko, "Opto-mechanical accelerometer based on strain sensing by a Bragg grating in a planar waveguide", *Sensors and Actuators A: Physical*, vol. 52, no. 1-3, pp. 25-32, 1996. Available: 10.1016/0924-4247(96)80121-x.

[37] K. Zandi, J. Belanger and Y. Peter, "Design and Demonstration of an In-Plane Silicon-on-Insulator Optical MEMS Fabry–Pérot-Based Accelerometer Integrated With Channel Waveguides", *Journal of Microelectromechanical Systems*, vol. 21, no. 6, pp. 1464-1470, 2012. Available: 10.1109/jmems.2012.2211577